

Design & Implementation of an Electric Fixed-wing Hybrid VTOL UAV for Asset Monitoring

Sarvesh Sonkar¹ , Prashant Kumar² , Yuvaraj Tanjore Puli³ , Riya Catherine George^{4,*} , Deepu Philip⁵ , Ajoy Kanti Ghosh² 

1. Indian Institute of Technology Kanpur  – Design – Kanpur/Uttar Pradesh – India. **2.** Indian Institute of Technology Kanpur  – Aerospace Engineering – Kanpur/Uttar Pradesh – India. **3.** GAIL (India) Limited  – Noida/Uttar Pradesh – India. **4.** Hiroshima University  – Civil and Environmental Engineering – Higashi Hiroshima/Hiroshima – Japan. **5.** Indian Institute of Technology  – Industrial Management and Engineering – Kanpur/Uttar Pradesh – India.

*Correspondence author: riyacgeorge@gmail.com

ABSTRACT

Fixed-wing unmanned aerial vehicles (UAVs) offer the best aerodynamic efficiency required for long-distance or high-endurance applications, albeit their runway requirement for take-off and landing in comparison with quadcopters, helicopters, and flapping-wing UAVs that can perform vertical take-off and landing (VTOL). Integrating a multirotor system with a fixed-wing UAV imparts VTOL capabilities without significantly compromising fixed-wing aerodynamic efficiency, endurance, payload capacity or range. Documented system design approaches to address various challenges of such fusion processes are sparse. This research proposes a holistic approach for designing, prototyping, and testing an electric-powered fixed-wing hybrid VTOL UAV. The proposed system design approach augments the standard aircraft design process with additional steps to integrate VTOL capabilities. Separate fixed-wing and multirotor designs were derived from the frozen mission requirements, which were then fused. The process used simulation for modeling and evaluating alternatives for the hybrid UAV created using standard aircraft design equations. We prototyped and instrumented the final design to validate operational capabilities through test flights. Multiple flight trials identified the ideal combination of Lithium-Polymer (Li-Po) batteries for VTOL (8000mAh) and fixed-wing (14000mAh) modes to meet the endurance and range requirements. The redundant power supplies also increased the survivability chances of the hybrid UAV during failures.

Keywords: Hybrid; UAV; VTOL; BLDC; Fuselage; Aircraft design.

INTRODUCTION

UAVs are becoming popular in avenues like aerial photography, surveying, monitoring, border patrol, surveillance, etc. (Sonkar *et al.* 2020; 2021). Researchers identified applications of UAVs in precision agriculture, package delivery, disaster management, etc., to improve efficiency and commercial viability (Sun *et al.* 2016; Kumar *et al.* 2020).

Two types of UAV platforms, viz., (i) rotary-wing and (ii) fixed-wing, are famous for such applications (Ebeid *et al.* 2017; Zhang *et al.* 2021). Rotary-wing systems possess enhanced maneuverability (Matsumoto *et al.* 2010), vertical take-off and landing

Received: Dec 26, 2022 | Accepted: Mar 13, 2023

Section editor: Rodrigo Palharini 

Peer Review History: Single Blind Peer Review.



This is an open access article distributed under the terms of the Creative Commons license.

(VTOL) capability, and midair hovering ability during flight (Sonkar *et al.* 2020). However, their inefficient operational nature severely limits both endurance and range. In contrast, fixed-wing UAVs efficiently utilize power, resulting in longer endurance and better flying range (Bauersfeld *et al.* 2021).

However, their requirement for a runway or catapult launch/arrest system for take-off and landing restricts their operations to locations with such infrastructure. The recent concept of the hybrid UAV capable of VTOL is popular among the research community, while not very popular in real-world applications (McCormick 1999; Stone *et al.* 2008).

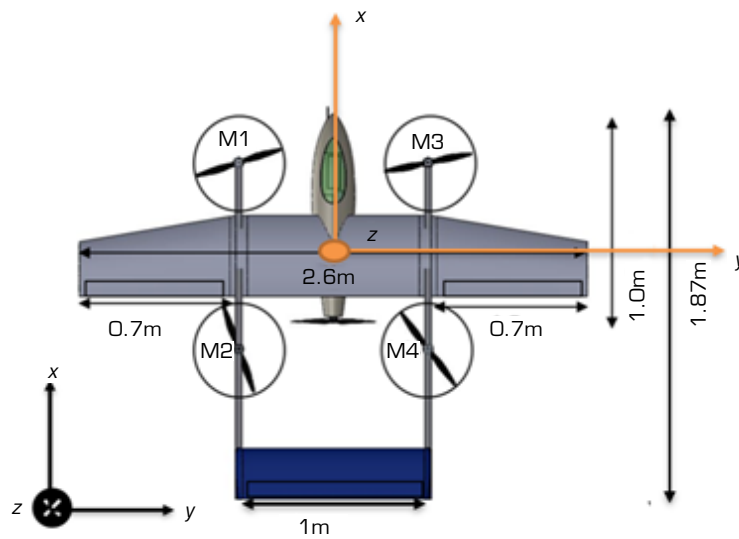
Combining features of both types result in tail-sitter (Lyu *et al.* 2017), tilt-rotor (Matsumoto *et al.* 2010), and hybrid VTOL UAVs (Wan *et al.* 2019). A tail-sitter UAV does its vertical climb on the empennage and then tilts the entire airframe horizontally for its level flight, accomplishing both tail-sitting and level flying using the same engines (Kubo and Suzuki 2008). But, the tilt-rotor UAVs only tilt their propulsion systems (motors) vertically and horizontally to achieve both take-off and forward flight, respectively (Bauersfeld *et al.* 2021). This research proposes an augmented, holistic approach based on the standard aircraft design process to design a hybrid VTOL UAV as a fusion of rotary and fixed-wing systems. This iterative process allows quickly processing of design alternatives and converges them to a viable design that can be flight tested.

Recently, electric propulsion applications for various transportation modes have increased significantly (Zong *et al.* 2021). Electric-powered fixed-wing UAV systems (Gur and Rosen 2009; Roskam 1985b) are becoming increasingly popular, with specific models being mass-produced. Small and medium-sized electric UAVs are gaining market popularity (Lyu *et al.* 2017), albeit having a much shorter range and endurance in comparison with the internal combustion engines (ICEs) propelled models (Ge *et al.* 2021; Oh *et al.* 2021). Existing technologies in Lithium-Ion (Li-Ion) and Lithium-Polymer (Li-Po) batteries allow energy densities up to 300-500 watt-hours/kg (Wh/kg) (Girishkumar *et al.* 2010). However, UAVs with ICEs burning aviation fuel offer more than 1400 Wh/kg (Cwojdzinski and Adamski 2014). While the theoretical limit of 370 Wh/kg for Li-Ion batteries is rapidly approaching (Li *et al.* 2017), two UAVs, viz., (i) “Zephyr” and (ii) “ALTI” demonstrated long endurances with energy densities between 350-380 Wh/kg (Rapinett 2009). Lithium-Sulfur (Li-S) and Lithium-Oxygen (Li-O) batteries offer futuristic promise with their theoretical energy densities of ~2570 and ~3500 Wh/kg, respectively (Luongo *et al.* 2009).

The electric motor is an essential component of electric propulsion. Lightweight brushless direct current (BLDC) electric motors under 360 kW are now available in the market (Jing *et al.* 2022). In the near future, small and medium electric UAVs will be able to compete with traditional ICE-powered UAVs (Xie *et al.* 2022). Simultaneously, multi-copter UAVs are gaining popularity due to maneuverability, controllability, and VTOL characteristics (Prouty 1995; Bhandari *et al.* 2017; Boon *et al.* 2017).

Multi-copter UAVs are easily manufacturable, with major sub-systems being a chassis, control board (autopilots), direct drive motors, batteries, and propellers. Simple alteration of the motor voltages can control the propeller rotation speed (RPM) (Çakici and Leblebicioğlu 2016). However, the high energy consumption of multi-copters results in shorter operational times. Alternatively, fixed-wing systems possess higher cruising efficiency (Garcia-Nieto *et al.* 2019), which translates to increased endurance and payload capacity.

The desire to combine the advantages of the fixed-wing and multi-copter systems resulted in the development of the hybrid VTOL system depicted in Fig. 1, which integrated the multi-copter propulsion into a conventional fixed-wing system. M1, M2, M3, and M4, in Fig. 1, represent the four vertical motors of the hybrid VTOL UAV. Such hybrid VTOL systems are ideal for aerial mapping, surveillance, and precise delivery applications. For example, small hand-launched fixed-wing UAVs such as PrecisionHawk Lancaster, senseFly eBee, and medium-sized catapult-launched UAVs like Penguin BE, currently dominate the aerial mapping and surveillance industry. We conducted multiple flight tests using the prototyped design of the final configuration to quantify range, endurance, and fail-safes. The payload integration occurred after such test flights established the design's robustness. Sonkar *et al.* (2022) have published the results of such experimental flights using the payload-integrated prototype.



Source: Elaborated by the authors.

Figure 1. 3-D model of the fixed-wing hybrid VTOL UAV.

Fixed-wing aircraft design relies heavily on methods that calculate the size, mass, and power requirements, where numerous well-known scaling techniques exist. Raymer (2018) introduced the first weight estimation method using the mission profile and a set of empirical equations for the ICE-powered aircraft. Earlier, McCormick (1999) created recommendations for the UAV mass breakdown and determined the battery mass percentage required for fixed-wing cruise flight of an electric fixed-wing UAV. Then, Bhandari *et al.* (2017) provided an integrated approach to assess the size of crewed electric fixed-wing aircraft. Zong *et al.* (2021) proposed a system for sizing heavy ICE-powered VTOL aircraft with maximum take-off weights (MTOW) of up to 27.5 tons. The designer's experience and suggestions from manufacturers primarily determine the propeller-motor combination. Recent research interests in commercial hybrid VTOL UAVs focus more on the control logic (Saeed *et al.* 2018). Researchers have reported a commercial hybrid VTOL UAV for medical applications with an MTOW of 25kg using ICE propulsion (Goetzendorf-Grabowski *et al.* 2021), which provided the impetus for the proposed design process of this research. This research also offers additional design process innovations like empennage modifications, boom-mount vertical propulsion, lightweight manufacturing process, etc.

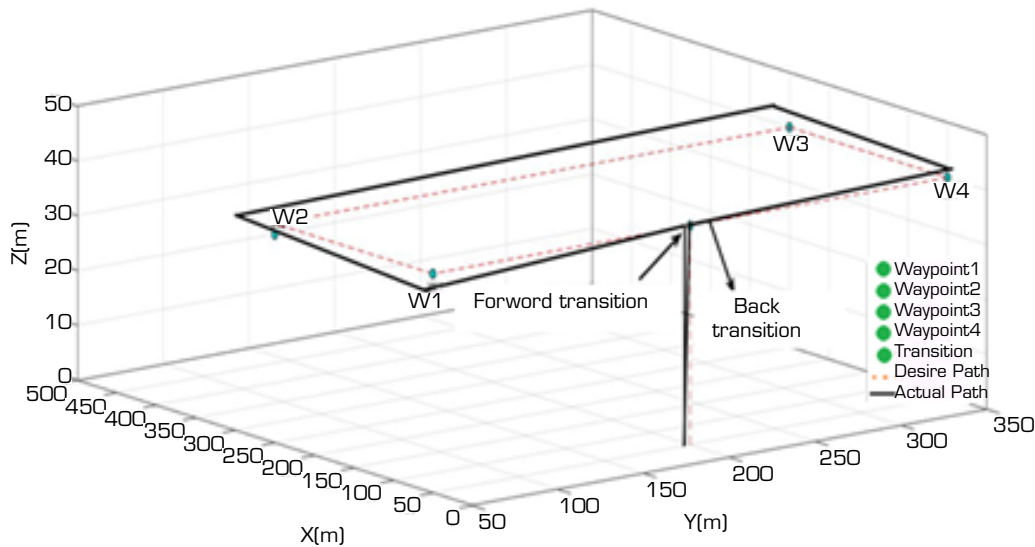
This research proposes an alternative design process for fixed-wing hybrid VTOL UAVs with electric propulsion. Creating separate and different designs for the fixed-wing and rotary-wing systems based on the mission and performance requirements becomes the preliminary step of our process, as explained in the airframe design section. Then, the selection and fusion of these designs occurred as the next step that created multiple realizations of the electric fixed-wing hybrid VTOL UAV. After selecting design(s) that fulfill the basic functionality requirements, design sizing of the wing, fuselage, tail, and control surfaces happened as part of the next step to attain optimal performance against specific choices of various components of UAV sub-systems. The designed hybrid UAV has five sub-systems, viz., (i) airframe (multirotor and fixed-wing), (ii) propulsion, (iii) control, (iv) communications, and (v) payload (camera and gas sensor). Specific component choices in each sub-system influence the overall system performance, requiring iterative re-design. The intended application of the designed fixed-wing hybrid VTOL UAV was natural gas pipeline monitoring along with onboard leakage detection. Our work also documents the evaluation of the configuration's efficiency, validation of the selected sizing/resizing technique, and testing of the control algorithms. The following sections first discuss the preliminary design, followed by the actual design of the experimental hybrid UAV. The final sections detail the testing and performance benchmarking.

Airframe design

This section describes the intended mission profile, which formed the foundation for designing the fixed-wing hybrid VTOL UAV. The intended usage of the UAV is monitoring natural gas pipelines with additional capability of leakage detection. Major subsections are mission requirements, wing, tail, fuselage designs and the VTOL section.

Mission requirements

The design space for the fixed-wing hybrid VTOL UAV's is a continuum created to conduct autonomous surveillance, asset monitoring and leakage detection of underground natural gas pipelines. The need to take off and land along the underground gas pipeline without runway infrastructure necessitates VTOL capability. Further, long pipeline stretches warrant extended operational ranges, which translates to extended endurance to cover such distances. A fixed-wing system's efficiency helps fulfill such endurance and range requirements. Thus, the categories identified from the mission requirements include weight, size, flying altitude, survivability, the need to combine the fixed-wing and rotary-wing systems, etc. The mission profile of the hybrid fixed-wing VTOL UAV has five main flight segments viz., (i) vertical take-off, (ii) forward transition (switch to quad mode from fixed-wing mode), (iii) cruise, climb, and loiter, (iv) back transition (switch from fixed-wing mode to quad mode), and (v) vertical landing as depicted in Fig. 2. Table 1 summarizes the initial design parameters derived from the mission requirements.



Source: Elaborated by the authors.

Figure 2. Mission Profile of Hybrid VTOL UAV.

Table 1. Hybrid UAV design parameters derived from the mission requirements

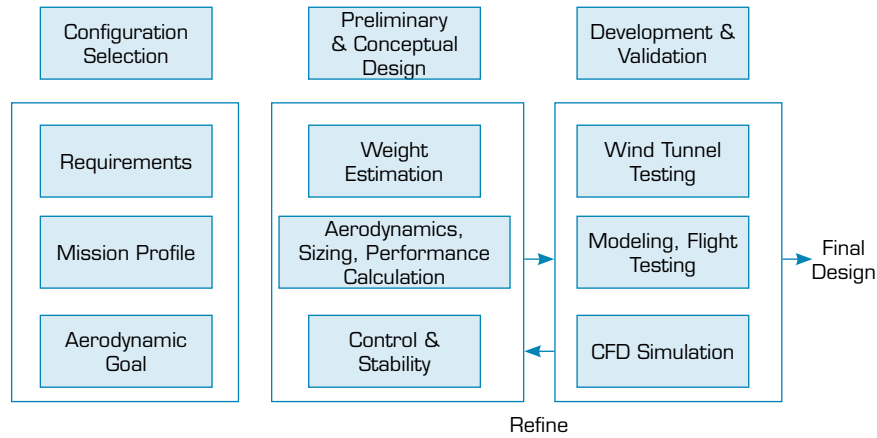
Maximum Take-Off Weight (MTOW)	< 12 kg
Payload capacity	<1.8 kg
Runway length for the take-off	0 m
Rate of ascend (multirotor mode)	2.5 m/s
Rate of descend (multirotor mode)	3.5 m/s
Climb rate in the fixed-wing mode	>2.5 m/s at Mean Sea Level (MSL)
Operational altitude (from take-off point)	200 m Above Ground Level (AGL)
Endurance	>45 min
Range	>20 km
Propulsion System	Electric Motors

Source: Elaborated by the authors.

Preliminary Design & Sizing

The preliminary design process focused on broadly identifying the weight, shape, and propulsion system from the mission requirements. Further, fine-tuning of these parameters using additional information about other sub-systems/components,

including various choices of BLDC motors, batteries, etc., helped finalize designs. Figure 3 illustrates the analytical process of the fixed-wing system design phase, having three sub-phases, viz., (i) configuration selection, (ii) conceptual design, and (iii) development and validation of the conceptual design. Figure 3 also depicts the iterative refinements made to the conceptual design between phases (ii) and (iii).



Source: Elaborated by the authors.

Figure 3. Design process of the fixed-wing hybrid VTOL UAV.

Identifying specific performance and mission requirements during phase (i) initiated the design process. We assumed that components viz., motors, propellers, and batteries that match the computed specifications are available in the market. First, we estimated the propulsion system's initial geometry, mass, thrust parameters, etc., followed by a numerical investigation similar to that of Oktay and Eraslan (2021) of the multirotor VTOL UAV propellers to determine the impact of airspeed and rotational speed on thrust coefficient. All these facilitated the selection of the actual models of BLDC motors, composite propellers, and Li-Po batteries for the hybrid UAV. Continuous updation of the hybrid UAV's MTOW occurred according to such choices of sub-systems.

WING DESIGN

Wing primarily generates the required lift for a fixed-wing aircraft along with drag and moment (nose down generally) simultaneously. Hence, factors such as performance requirements, stability, ease of control, manufacturability, system costs, flight safety, etc., are essential for wing design. Major performance requirements of the hybrid UAV include stall speed, maximum speed, range, and endurance. Körpe *et al.* (2019) presented the turbulence model to perform a numerical analysis of the impact of the dimensionless wall distance on the aerodynamic coefficient of an aerofoil. Next, longitudinal and lateral directional stability constitute the major stability requirements. Other parameters influencing the wing design process include wing area, airfoil selection, aspect ratio, taper ratio, tip chord, sweep angle, dihedral angle, incidence angle, aileron sizing, servo mounting position, etc. Size and weight constraints mainly limit the minimum wing size. We considered four different wing designs viz and after comparisons, we reached the following conclusions:

- Rectangular wing generates the lightest wing loading for the given constraints, resulting in the lowest lift coefficient (C_L) value for cruise flight. Further, the lift distribution pattern and substantial tip losses ruled out this design.
- Tapered wing provides better lift distribution than the rectangular wing. But, larger wing loading coupled with a higher C_L requirement for cruise makes this design less preferred.
- Elliptical wing offers the best lift distribution and negligible wing tip losses. However, this design also suffers from high wing loading C_L requirements and added manufacturing difficulty.
- Semi-tapered wing has similar lift distribution as that of a tapered wing while eliminating the need for wing tip modification to reduce tip losses. The wing loading is less than both tapered and elliptical wings, as the C_L required for the cruise is also less.

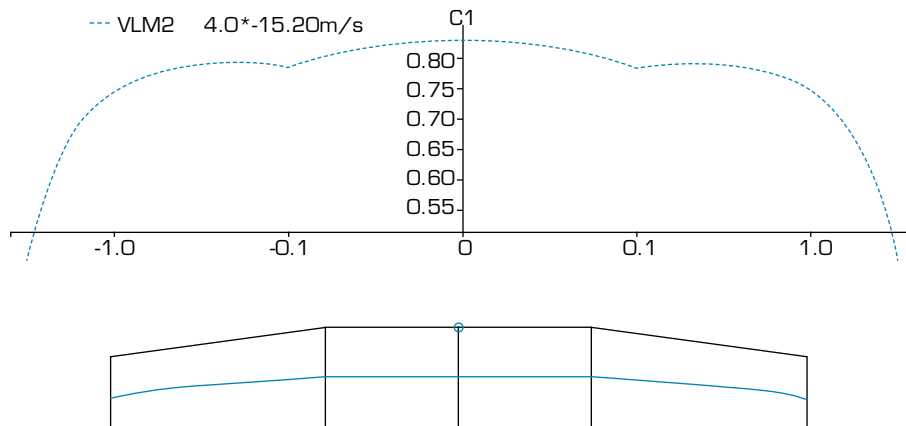
Though the research suggests that an elliptical wing offers better lift distribution with minimal drag, its manufacturing is costly and time-consuming. Further, the Reynolds Number towards the elliptical wing tip becomes relatively small, causing significant deviations in its lift estimations. Choosing the semi-tapered wing shown in Fig. 4, it resulted in a more straightforward design with better aerodynamic and structural advantages, as evaluated using the XFLR5 software. Further, the semi-tapered wing is relatively easy to fabricate and provides good lift distribution.



Source: Elaborated by the authors.

Figure 4. Wing geometry of the fixed-wing system in XFLR 5

XFLR5 is a design and analysis tool for wing, tail, and airfoils at low or high Reynolds numbers (Dwivedi *et al.* 2020). Figure 5 depicts the resulting elliptical lift distribution curves after using the Horseshoe Vortex method for estimating lift in XFLR5. The final wing design resulted in a span of 2.6m, wing area of 0.9m², mean aerodynamic chord of 0.35m, and cruise speed of 17m/s. We conclude from Fig. 5 that the lift is maximum at the root chord and minimum at the tip chord of the wing. Specific attention during design avoided the over-tapering of the wing, thereby eliminating its associated complications. A strong taper of the wing causes the local lift coefficient, $C_L(wing)$, to have a maximum value near the root (Fig. 5), creating the adverse possibility of tip stall during flight. Moreover, it also causes small chords Reynolds Number near the tip, thereby reducing the maximum achievable C_L of the wing. Wing loading is the ratio of the aircraft's MTOW to its wing area, which is a critical parameter of the fixed-wing aircraft design.

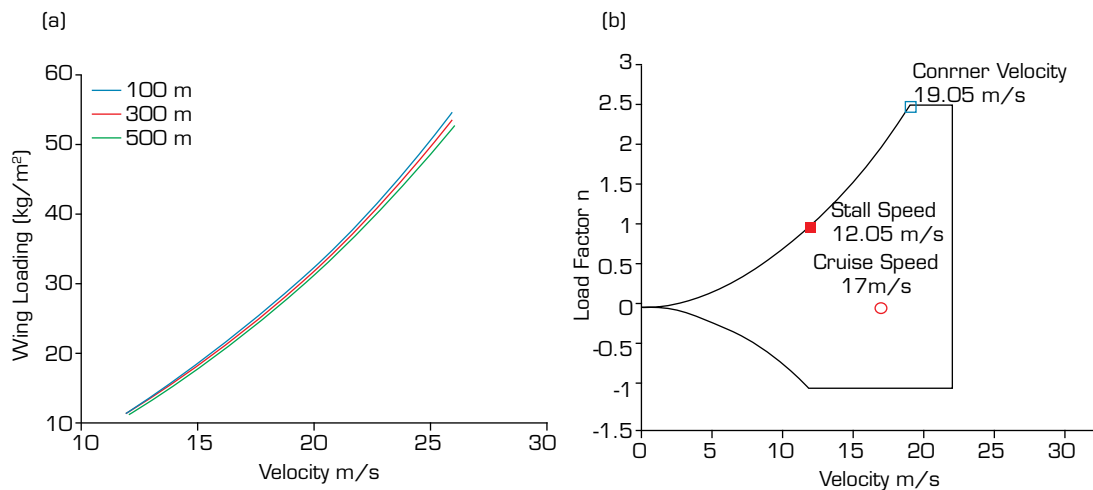


Source: Elaborated by the authors.

Figure 5. Lift distribution along the wing estimated using XFLR5.

Figure 6a shows the wing loading while operating at the maximum lift coefficient ($C_{L,Max}$) for various altitudes, viz., 100, 300, and 500 meters. Factors like the UAV wing's size, shape, and attachment angle on the fuselage determine its take-off and landing performance, stall speed, and maneuverability. Greater wing loading helps to maintain smaller wing sizes with respect to the aircraft's mass. If all other factors remain constant, the UAV with smaller wings will have a lower stall speed (making it quicker at cruising speed) than one with larger wings. In addition, UAVs with greater wing loading will be more stable in steady flight than those with lower wing loading.

The mission requirements mandate a low cruise speed (about 16-18 m/s), thereby freezing the maximum wing loading for a given stall speed (estimated around 18-20 kg/m²), and determining the wing sizing. Also, researchers advise maintaining wing loading that realizes nearly 20% structural safety (Roskam 1985b). Figure 6b depicts the V-n diagram that plots the load factor against the velocity. Maintaining lower loiter or cruise speeds are generally advised to lower the dynamic pressure, thus generating lesser loads on the structure. Lower wing loading helps achieve lower stall velocity, resulting in lower cruise speed. We can achieve lower wing loading by reducing the weight for a given wing area, which in turn results in a load lower than the usual on the wing during maneuver ($L = nW$, where n is the load factor).



Source: Elaborated by the authors.

Figure 6. (a) Wing loading vs. velocity for fixed-wing design at ($C_{(L,max)}$) for different altitudes; (b) V-n diagram.

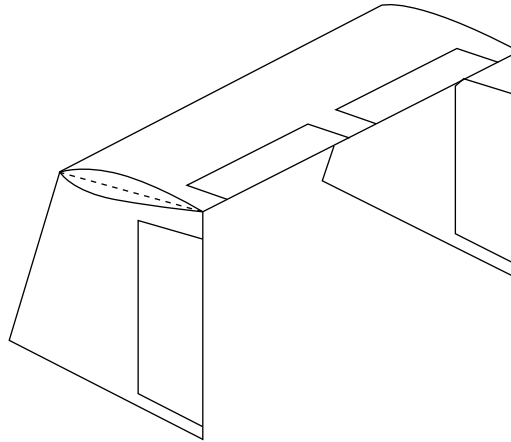
The wing incidence angle is the pitch angle of the wing to the fuselage. In the case of an untwisted wing, it is simply the angle between the airfoil chord line and the fuselage reference line. Usually, minimization of drag during cruise flight drives the choices of wing incidence angle. This implies that when the wing is at the desired angle of attack (AOA) for the chosen design condition, the fuselage is at the AOA that minimizes the total drag.

TAIL GEOMETRY AND SIZING

The tail provides stability to the UAV. Zero-loaded tails are usually preferred so that the lift coefficient for the designed configuration is zero, thereby keeping the induced drag zero. Numerous tail configurations exist identical to that of the manned aircraft that can have single or multiple attachment points. Before finalizing the tail configuration, we compared the advantages and disadvantages of major tail designs reported in the literature, like U, inverted U, V, inverted V, T, inverted T, H, etc.

Both U and inverted U tails possess the same number of surfaces, viz., two vertical and one horizontal. Further, both tail designs do not obstruct the wing downwash, prop wash, wakes, and vortices. However, they suffer from a destabilizing effect at higher AOAs as aerodynamic loads on the horizontal tail get transferred to the vertical tails and booms. Additional strengthening of the vertical tails solves this issue but increases the total weight. H-tail design has one horizontal surface between two vertical tails, combining the advantages while eliminating the disadvantages of both U and inverted U tails. However, careful determination of the relative location of the horizontal tail is necessary to negate any deep stall, thereby making the design process more complex. The added weight due to additional strengthening further makes this design costly. Finally, both V and inverted V-tails have only two slanted surfaces that realize the same functions as the elevator and rudder of a conventional tail configuration, thereby reducing the drag and weight. Conversely, its control system is more complex due to the simultaneous occurrence of elevator and rudder components during various maneuvers compared with other configurations.

We chose the inverted U-tail design with a pusher configuration for the fixed-wing UAV design, having a twin-boom connection to the fuselage. Figure 7 depicts the tail design, including the tiny tappers on the vertical control surfaces. Both horizontal and vertical tail sections of Table 3 summarize the principal design parameters of both surfaces. The simplicity of this design resulted in better manufacturability, maintainability, and overall efficiency. Further, the horizontal tail tends to provide more drag and stabilizing effects at high angles of attack. The structural heaviness and its associated marginal costs vastly outnumbered the benefits of this design.



Source: Elaborated by the authors.

Figure 7. Tail Design.

FUSELAGE DESIGN

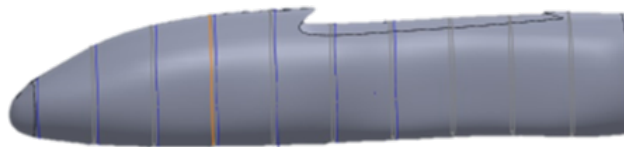
Fuselage design is a complicated process involving several factors like payload capacity, avionics, battery sizes, propulsion, and other parameters depending upon the UAV's applications. Hence, we used the guidelines of Roskam (1985a) and Nelson (1989) to analyze the design parameters. We chose a simple symmetric fuselage geometry and analyzed it to obtain a rough estimate of the pitching moment due to the fuselage at an AOA $(C_{(m_\alpha)_f})$ and pitching moment with zero AOA $(C_{(m_0)_f})$. Throughout the design iterations, Eqs. 1 and 2 facilitated the revision of fuselage geometries and the corresponding values of $(C_{(m_\alpha)_f})$ and $(C_{(m_0)_f})$ respectively (Roskam 1985b). Figure 8 indicates the oval shape of the UAV's fuselage, which also integrates two square hollow tubes to facilitate the attachment of the tail booms. Table 2 compiles all major fuselage specifications of the hybrid UAV. Since the intended application of the UAV is surveillance, reconnaissance, and asset monitoring, the primary payload consists of a gas sensor and a gimbal camera. These payload considerations also determined the access points location along with the width and length of the fuselage.

$$(C_{m_\alpha})_f = \frac{(K_2 - K_1)}{36.5S\bar{c}} \sum_{x=0}^{x=lf} W^2 f(\alpha_{0w} + i_f) \Delta x \quad (1)$$

$$C_{m_0f} = \frac{1}{36.5S\bar{c}} \sum_{x=0}^{x=lf} \frac{W^2 f(\partial \epsilon_u)}{\partial \alpha} \Delta x \quad (2)$$

Where:

S = wing reference area; \bar{c} = wing mean aerodynamic; w_f = average width of fuselage section; Δx = length of fuselage increment; A_{0w} = wing zero lift angle relative to fuselage ref. line in degrees (-4°); i_f = incidence of the fuselage camber line relative to the fuselage reference line at the centre of each fuselage increment; $K_2 - K_1$ is the correction factor used for designing the overall shape of a streamlined body (fixed-wing hybrid VTOL UAV); $(\delta_{\epsilon_u})/\delta$ = change in local flow angle with angle of attack.



Source: Elaborated by the authors.

Figure 8. 3D Fuselage Design.

Table 2. Fuselage Specifications.

Parameter	Symbol	Values
Length of fixed-wing UAV(m)	L_0	1.78m
Length of the cockpit(m)	$L_{cockpit}$	1.0m
Max width of the cockpit(m)	$W_{cockpit}$	0.15m
Max width of the tail boom(m)	W_{boom}	0.025m
Fuselage depth	d	0.17m
Fuselage side area(m ²)	S_{f_u}	0.1438sq.m
Fuselage pitching moment Coeff. at $\alpha = 0$	$(C_{m_o})_f$	-0.0178

Source: Elaborated by the authors.

DESIGN SUMMARY AND CHARACTERISTICS

This section summarizes the complete UAV geometry by compiling all pertinent information from the previous sections. Standard values published in textbooks and documents helped in sizing the control surfaces. The validation and verification of the geometry occurred through necessary parameter estimations, and stability and control derivatives while making iterative design changes. Fixed-wing systems efficiently recover from stall during forward flight by lowering the nose to gain airspeed. The presence of the independent quadcopter VTOL system provides an additional safety net.

Further, the separate VTOL system can slow the fixed-wing flight to hover, providing an added benefit. Table 3 summarizes the fixed-wing hybrid VTOL UAVs' primary design and control parameters in five parts. The first part tabulates the major mission-related and physical parameters, while the second details the wing-related parameters. The third and fourth parts of Table 3 contain the horizontal and vertical tail parameters, respectively. The last part of Table 3 summarizes the parameters for the independent rotary-wing VTOL section.

Table 3. Full Parameter List of the Fixed-wing Hybrid VTOL UAV.

Parameter	Hybrid UAV
Total Weight of Aircraft (kg)	12
Cruise Velocity of Aircraft (m/s)	17~18
Ambient Air Density (kg/m ³)	1.2
Position of Centre of Mass w.r.t. wing L.E. (m)	0.131
Position of Neutral point w.r.t. wing L.E. (m)	0.205
Wingspan (m)	2.6
Length of wing root chord (m)	0.38
Length of wing tip chord (m)	0.27
Wing	
Wing Airfoil	E-214
Wing Setting angle (deg.)	0
Sweep of wing mid-chord points (deg.)	0

Continue...

Table 3. Continuation.

Parameter	Hybrid UAV
Lift at zero angle of attack	0.3260
Setting angle of Wing	0
Aileron span (m)	0.8
Aileron chord (m)	0.085
Horizontal Tail	
Horizontal Stabilizer Span (m)	1
Length of horizontal stabilizer root chord (m)	0.18
Length of horizontal stabilizer tip chord (m)	0.18
Horizontal Stabilizer airfoil	NACA0012
Tail setting angle (deg.)	≈-2
Length of the horizontal tail arm (m)	1.09
Horizontal tail volume efficiency	0.6
Elevator span (m)	0.92
Elevator chord (m)	0.06
Vertical Tail	
Vertical Stabilizer Span (m)	0.2
Length of vertical stabilizer root chord (m)	0.22
Length of vertical stabilizer tip chord (m)	0.18
Vertical Stabilizer airfoil	NACA0012
Sectional lift curve slope of vertical stabilizer airfoil	5.9689
Rudder span (m)	0.16
Rudder chord (m)	0.06
Length of vertical tail arm (m)	1.06
Vertical tail volume efficiency	≈0.04
Vertical Thrusters	
M1, M2, M3, M4 Weights (kg)	1.2
Distance between M1, M2 and M3, M4(axial) (m)	0.94
Distance between M1, M2 and M3, M4(Parallel) (m)	1

Source: Elaborated by the authors.

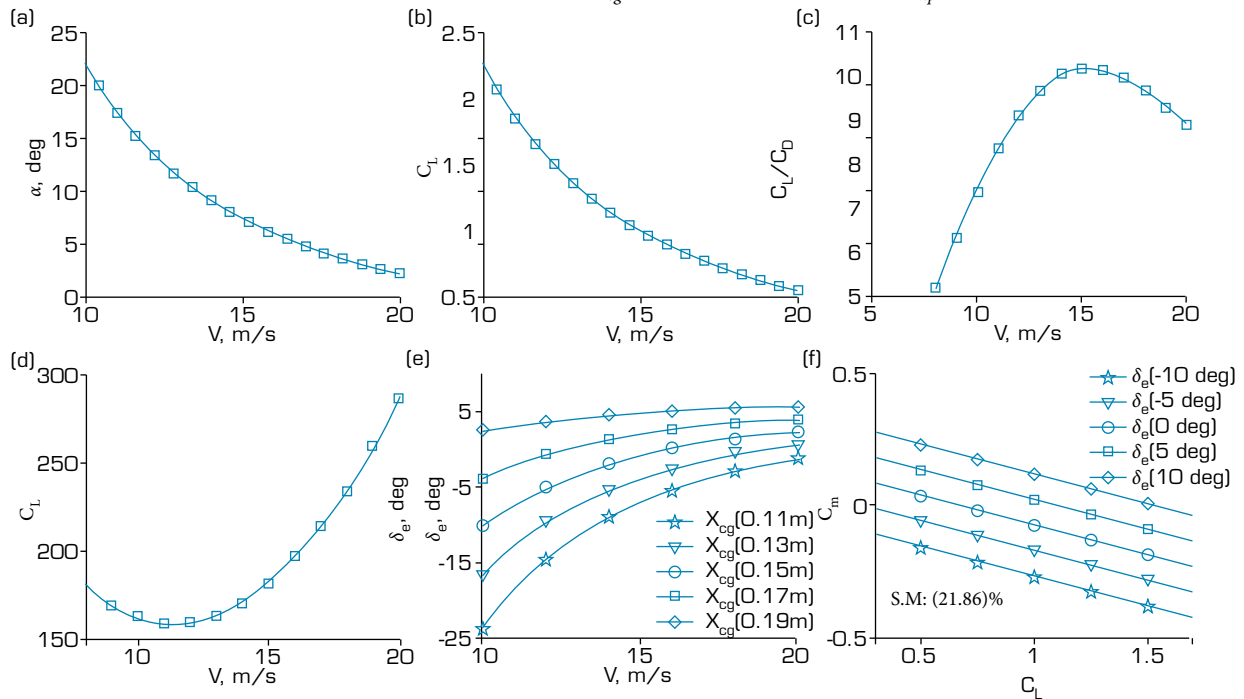
Now, we document the performance testing of the prototyped fixed-wing hybrid VTOL UAV. Table 4 details the exact physical parameters of the prototype having a wing area of 0.88 m², a wingspan of 2.6m, and a mean aerodynamic chord of 0.34m. Figure 1 indicates that the x-axis is in the forward direction along the nose, the y-axis is along the wing, and the z-axis is facing downwards. I_{xx} , I_{yy} , I_{zz} & I_{xz} . Together, they represent the moment of inertia values of the system about the x, y, and z-axis. Calculating the moment of inertia utilized the 3D CAD model of the fixed-wing hybrid VTOL UAV. The values of I_{xy} , I_{yz} were negligible and, hence, taken as zero.

Table 4. Physical Parameters of the fixed-wing hybrid VTOL UAV.

Parameter	Value
Mass	12 Kg
MAC	0.34 m
Wingspan	2.6 m
Area	0.87 m ²
I_{xx}	3.551 kgm ²
I_{yy}	4.4221 kgm ²
I_{zz}	7.4841 kgm ²
I_{xz}	0.1274 kgm ²

Source: Elaborated by the authors.

Four main performance parameters measured from test flights include (i) trim velocity, (ii) trim AOA, (iii) aerodynamic efficiency (L/D), and (iv) elevator trim (δ_e). The estimation of range and required power depends on these parameters. Figure 9 compares the performance plots of the fixed-wing hybrid VTOL UAV prototype. As observed from Fig. 9a, the trim AOA is approximately 4.5 degrees, and the lift coefficient at the trim C_{Ltrim} . The condition is 0.6877 from Fig. 9b. Further, Fig. 9c and d provide the aerodynamic efficiency and power required at trim conditions. Figure 9e depicts the elevator needed to trim the UAV, which indicates the required elevator values at the UAV's center of gravity (CoG) to determine elevator deflection limits. The CoG locations of elevator deflections are about the wing's leading edge reference line shown in Fig. 4. Thus, Fig. 9e allows the checking of the elevator limits against CoG location for different airspeeds. Since the elevator can deflect between +6 to -25 degrees in either direction from the trim conditions, Fig. 9e also helps to determine the forward and backward limits of CoG. Figure 9f plots the relation between the pitching moment (C_m) and the lift coefficient (C_L) for different elevator deflections at $X_{cg} = 0.131m$ and neutral point $X_{np} = 0.205m$, as reported in Table 3.



Source: Elaborated by the authors.

Figure 9. performance plots for VTOL UAV (a) angle of attack α (b) Lift coefficient (C_L) (c) Aerodynamic efficiency (C_L/C_D) (d) Power Required (P_R) (e) Elevator required (δ_e) versus velocity with CoG variation (f) Pitching moment versus lift coefficient with elevator variation.

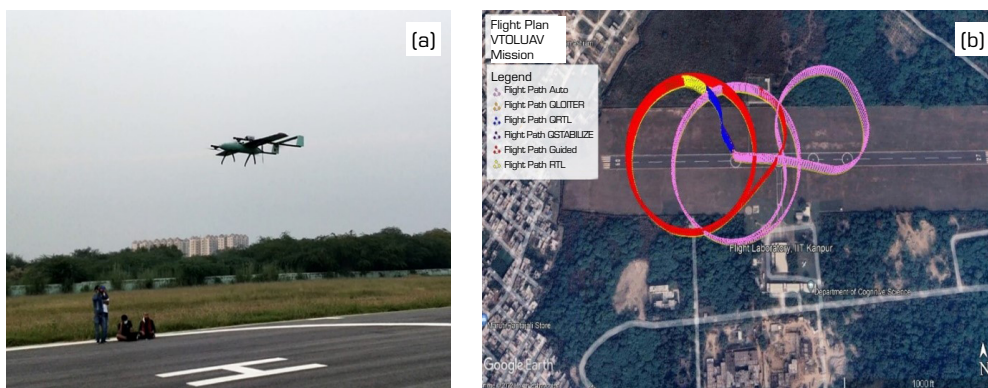
Table 5 compiles the prototype's multiple test flights with various Li-Po battery combinations. The second and third columns of Table 5 provide the VTOL and fixed-wing endurance in minutes, respectively, for a specific Li-Po battery combination. The information contained within curly braces in the second and third columns identifies the number of cells (resultant voltage) and energy stored in the particular battery. The fourth column combines the VTOL and fixed-wing flight times, while the last column details the intended application of the UAV configuration. Flight tests eight and nine suggested that similar total endurance is possible with a 40% lighter VTOL battery (8,000 mAh) while keeping the same 14,000 mAh battery for the fixed-wing flight.

Table 5. Flight times and endurance with different combinations of Li-Po Battery.

Test Flight	Rotary-wing VTOL endurance for different battery options	Fixed-wing flight-time for different battery options	Total flight time of the hybrid VTOL UAV	Application
1	{5.25min}, {2x6S,5500mAh}	{17min}, {6S,6000mAh}	22.5min	Surveillance, encroachment detection
2	{6min}, {2x6S,6000mAh}	{22min}, {6S,8000mAh}	28min	Surveillance, encroachment detection
3	{8.2min}, {2x6S,8000mAh}	{33min}, {6S,10000mAh}	41.2min	Surveillance, gas-leak detection
4	{9.3min}, {2x6S,9000mAh}	{28min}, {6S,9000mAh}	41.2min	Mapping, encroachment detection
5	{10.4min}, {2x6S,10000mAh}	{28min}, {6S,9000mAh}	37.3min	Mapping
6	{6min}, {2x6S,6000mAh}	{33min}, {6S,10000mAh}	39min	Surveillance, gas-leak detection
7	{6min}, {2x6S,6000mAh}	{53min}, {6S,14000mAh}	58min	Surveillance, gas-leak detection
8	{8.2min}, {2x6S,8000mAh}	{53min}, {6S,14000mAh}	61.2min	Surveillance, gas-leak detection
9	{10.4min}, {2x6S,10000mAh}	{53min}, {6S,14000mAh}	63.4min	Surveillance, gas-leak detection

Value is { }, { } shows the endurance timing in minutes and lipo battery capacity, respectively. Source: Elaborated by the authors.

Figure 10a illustrates the mission plan displayed on the ground control station (GCS), including two loiters during the flight test. The flight plan consistently subjected the hybrid UAV prototype to various maneuvers along with shorter duration level flights, estimating a reasonably worst-case endurance. It also facilitated the stress test of the control surfaces. Next, Fig. 10b captures the flight of the hybrid UAV high-density foam (HDF) prototype in the VTOL mode.



Source: Elaborated by the authors.

Figure 10. Flight testing (a) Mission plan from the GCS (b) Actual VTOL flight of the HDF prototype.

CONCLUSION

This research documents the analytical design, analysis, prototyping, and performance flight testing of a fixed-wing hybrid VTOL UAV with four vertical thrusters (rotary-wing) and one pusher (fixed-wing) propulsion. This research was motivated by the existing lacuna in design approaches for hybrid UAVs that integrate fixed-wing and quadcopter (rotary-wing) systems. First, we iteratively determined the hybrid UAV's overall geometry and aerodynamic design for the desired speed and endurance. The entire airframe has three parts, viz., (i) wing, (ii) tail, and (iii) fuselage. Wing design focused on lift distribution and wing loading analysis. Next, we documented the selection approach of the inverted 'U' tail geometry. Finally, standard design equations facilitated the fuselage design to carry specialized payloads. Table 3 summarizes the final design parameters of the resultant fixed-wing hybrid VTOL UAV. Then, we prototyped the fixed-wing hybrid VTOL UAV using HDF, which got instrumented with autopilot, batteries, propulsion units, communication, and payloads. Multiple test flights of the prototyped UAV allowed us to quantify the actual endurance, airspeed, and mission capabilities for different battery combinations, thereby evaluating the design's performance. The combination of an 8,000 mAh battery for VTOL and a 14,000 mAh battery for cruise delivered the desired endurance of 60 minutes with sufficient power remaining in both batteries. Thus, the proposed approach provides a simpler alternative for the quick design and development of a fixed-wing hybrid UAV with VTOL capabilities.

CONFLICT OF INTEREST

There is no conflict of interest.

AUTHORS' CONTRIBUTION

Conceptualization: Sonkar S; Kumar P; Ghosh AK; Philip D; Puli YT; **Methodology:** Sonkar S; Kumar P; Ghosh AK; **Software:** Sonkar S; Kumar P; **Validation:** Sonkar S; Kumar P; **Formal analysis:** Sonkar S; Kumar P; **Investigation:** Sonkar S; Kumar P; Philip D; **Resources:** Sonkar S; Kumar P; Philip D; Puli YT; **Data Curation:** Sonkar S; Kumar P; Philip D; **Visualization:** Sonkar S; Kumar P; Philip D; **Supervision:** Philip D; Ghosh AK; George RC; **Project administration:** Philip D; **Funding acquisition:** Philip D; **Writing – Original Draft:** Sonkar S; **Writing – Review & Editing:** Philip D; George RC.

DATA AVAILABILITY STATEMENT

Some or all data used in this study are owned by the funding agency and may only be provided with restrictions.

FUNDING

This project was funded by Gas Authority of India Limited.

ACKNOWLEDGEMENTS

Not applicable

REFERENCES

- Bauersfeld L, Spannagl L, Ducard GJJ, Onder CH (2021) MPC Flight Control for a Tilt-Rotor VTOL Aircraft. *IEEE Trans Aerosp Electron Syst* 57(4):2395-2409. <https://doi.org/10.1109/TAES.2021.3061819>
- Bhandari S, Navarro P, Ruiz A (2017) Flight Testing, Data Collection, and System Identification of a Multicopter UAV. Paper presented AIAA Modeling and Simulation Technologies Conference. AIAA Sci Tech Forum: Grapevine, Texas. <https://doi.org/10.2514/6.2017-1558>
- Boon MA, Drijfhout AP, Tesfamichael S (2017) Comparison of a fixed-wing and multi-rotor UAV for environmental mapping applications: A case study. *Int. Arch. Photogramm Remote Sens Spatial Inf Sci* 42:47-54. <https://doi.org/10.5194/isprs-archives-XLII-2-W6-47-2017>
- Çakici F, Leblebicioğlu MK (2016) Control System Design of a Vertical Take-off and Landing Fixed-Wing UAV. *IFAC-PapersOnLine* 49(3):267-272. <https://doi.org/10.1016/j.ifacol.2016.07.045>
- Cwojdzński L, Adamski M (2014) Power units and power supply systems in UAV. *Aviation* 18(1):1-18. <https://doi.org/10.3846/16487788.2014.865938>
- Dwivedi YD, Waykar TMS, Varun L (2020) Aerodynamic Characterization Of Albatross-Inspired Airfoils/Wings. *Int J Adv Sci Technol* 29(12s):801-815.
- Ebeid E, Skriver M, Jin J (2017) A Survey on Open-Source Flight Control Platforms of Unmanned Aerial Vehicle. Paper presented 2017 Euromicro Conference on Digital System Design (DSD). IEEE: Vienna, Austria. <https://doi.org/10.1109/DSD.2017.30>
- Garcia-Nieto S, Velasco-Carrau J, Paredes-Valles F, Salcedo JV, Simarro R (2019) Motion equations and attitude control in the vertical flight of a VTOL bi-rotor UAV. *Electronics* 8(2):208. <https://doi.org/10.3390/electronics8020208>
- Ge J, Liu L, Dong X, He Y (2021) A trajectory optimization method for reducing magnetic disturbance of an internal combustion engine powered unmanned aerial vehicle. *Aerosp Sci Technol* 116:106885. <https://doi.org/10.1016/j.ast.2021.106885>
- Girishkumar G, McCloskey B, Luntz AC, Swanson S, Wilcke W (2010) Lithium-Air Battery: Promise and Challenges. *J Phys Chem Lett* 1(14):2193-2203. <https://doi.org/10.1021/jz1005384>
- Goetzendorf-Grabowski T, Tarnowski A, Figat M, Mieloszyk J, Hernik B (2021) Lightweight unmanned aerial vehicle for emergency medical service – Synthesis of the layout. *Proc Inst Mech Eng G J Aerosp Eng* 235(1):5-21. <https://doi.org/10.1177/0954410020910584>
- Gur O, Rosen A (2009) Optimizing Electric Propulsion Systems for Unmanned Aerial Vehicles. *J Aircr* 46(4):1340-1353. <https://doi.org/10.2514/1.41027>
- Jing L, Tang W, Wang T, Ben T, Qu R (2022) Performance Analysis of Magnetically Geared Permanent Magnet Brushless Motor for Hybrid Electric Vehicles. *Trans Transp Electrification* 8(2):2874-2883. <https://doi.org/10.1109/TTE.2022.3151681>
- Körpe DS, Kanat ÖÖ, Oktay T (2019) The Effects of Initial γ plus: Numerical Analysis of 3D NACA 4412 Wing Using γ -Re θ SST Turbulence Model. *EJOSAT* 17:692-702. <https://doi.org/10.31590/ejosat.631135>
- Kubo D, Suzuki S (2008) Tail-Sitter Vertical Takeoff and Landing Unmanned Aerial Vehicle: Transitional Flight Analysis. *J Aircr* 45(1):292-297. <https://doi.org/10.2514/1.30122>

- Kumar P, Sonkar S, Ghosh AK, Philip D (2020) Real-time vision-based tracking of a moving terrain target from Light Weight Fixed Wing UAV using gimbal control. Paper presented 2020 7th International Conference on Control, Decision and Information Technologies (CoDIT). IEEE: Prague, Czech Republic. <https://doi.org/10.1109/CoDIT49905.2020.9263896>
- Li Y, Yang J, Song J (2017) Design principles and energy system scale analysis technologies of new lithium-ion and aluminum-ion batteries for sustainable energy electric vehicles. *Renew Sust Energ Rev* 71:645-651. <https://doi.org/10.1016/j.rser.2016.12.094>
- Luongo CA, Masson PJ, Nam T, Mavris D, Kim HD, Brown GV, Waters M, Hall D (2009) Next generation more-electric aircraft: A potential application for HTS superconductors. *IEEE Trans Appl Supercond* 19(3):1055-1068. <https://doi.org/10.1109/TASC.2009.2019021>
- Lyu X, Gu H, Wang Y, Li Z, Shen S, Zhang F (2017) Design and implementation of a quadrotor tail-sitter VTOL UAV. Paper presented 2017 IEEE International Conference on Robotics and Automation (ICRA). IEEE: Singapore. <https://doi.org/10.1109/ICRA.2017.7989452>
- Matsumoto T, Kita K, Suzuki R, Oosedo A, Go K, Hoshino Y, Konno A, Uchiyama M (2010) A hovering control strategy for a tail-sitter VTOL UAV that increases stability against large disturbance. Paper presented 2010 IEEE International Conference on Robotics and Automation. Anchorage, United States. <https://doi.org/10.1109/ROBOT.2010.5509183>
- McCormick BW (1999) *Aerodynamics of V/STOL flight*. North Chelmsford: Courier Corporation.
- Nelson RC (1989) *Flight Stability and Automatic Control*. New York: WCB/McGraw Hill.
- Oh S, Park C, Nguyen D, Kim S, Kim Y, Choi Y, Lee J (2021) Investigation on the operable range and idle condition of hydrogen-fueled spark ignition engine for unmanned aerial vehicle (UAV). *Energy* 237:121645. <https://doi.org/10.1016/j.energy.2021.121645>
- Oktay T, Eraslan Y (2021) Numerical Investigation of Effects of Airspeed and Rotational Speed on Quadrotor UAV Propeller Thrust Coefficient. *J Aviat* 5(1):9-15. <https://doi.org/10.30518/jav.872627>
- Prouty RW (1995) *Helicopter performance, stability, and control*. Malabar: Krieger Publishing.
- Rapinett A (2009) *Zephyr: A High Altitude Long Endurance Unmanned Air Vehicle*. (doctoral dissertation). Surrey: University of Surrey. In English.
- Raymer DP (2018) *Aircraft Design: A Conceptual Approach, Sixth Edition*. Reston: AIAA. <https://doi.org/10.2514/4.104909>
- Robotics and Automation. Anchorage, United States. <https://doi.org/10.1109/ROBOT.2010.5509183>
- Roskam J (1985a) *Airplane design*. Lawrence: DARcorporation.
- Roskam J (1985b) *Airplane Design Part VII: Determination of Stability, Control and Performance Characteristics*. Lawrence: DARcorporation.
- Saeed AS, Younes AB, Cai C, Cai G (2018) A survey of hybrid Unmanned Aerial Vehicles. *Prog Aerosp Sci* 98:91-105. <https://doi.org/10.1016/j.paerosci.2018.03.007>
- Sonkar S, Kumar P, Philip D, Ghosh AK (2020) Low-Cost Smart Surveillance and Reconnaissance Using VTOL Fixed Wing UAV. Paper presented 2020 IEEE Aerospace Conference. IEEE: Big Sky, United States. <https://doi.org/10.1109/AERO47225.2020.9172554>
- Sonkar S, Kumar P, Philip D, Ghosh AK (2021) Real-Time Video Processing System for Fixed-Wing UAV. Paper presented Proceedings of the International Conference on Optics and Electro-Optics. Springer: Dehradun, India. https://doi.org/10.1007/978-981-15-9259-1_67

- Sonkar SK, Kumar P, George RC, Philip D, Ghosh AK (2022) Detection and Estimation of Natural Gas Leakage Using UAV by Machine Learning Algorithms. *IEEE Sens J* 22(8):8041-8049. <https://doi.org/10.1109/JSEN.2022.3157872>
- Stone RH, Anderson P, Hutchison C, Tsai A, Gibbens P, Wong KC (2008) Flight Testing of the T-Wing Tail-Sitter Unmanned Air Vehicle. *J Aircr* 45(2):673-685. <https://doi.org/10.2514/1.32750>
- Sun J, Li B, Jiang Y, Wen C-Y (2016) A Camera-Based Target Detection and Positioning UAV System for Search and Rescue (SAR) Purposes. *Sensors* 16(11):1778. <https://doi.org/10.3390/s16111778>
- Wan AN, Sim GMS, Koh RWL, Koh RKF, Teo GT, Yap TH, Nilju T, Srigrarom S, Holzapfel F, Marvakov V, Bhadwaj P, Tantrairatn S, Sakulthong S (2019) Development of UGS-TUM Vertical Take off Landing (VTOL) Drone with Flight Control. Paper presented 2019 1st International Symposium on Instrumentation, Control, Artificial Intelligence, and Robotics, ICA-SYMP. IEEE: Bangkok, Thailand. <https://doi.org/10.1109/ICA-SYMP.2019.8646176>
- Xie Y, He S, Savvaris A, Tsourdos A, Zhang D, Xie A (2022) Convexification in energy optimization of a hybrid electric propulsion system for aerial vehicles. *Aerosp Sci Technol* 123:107509. <https://doi.org/10.1016/j.ast.2022.107509>
- Zhang H, Wang L, Tian T, Yin J (2021) A Review of Unmanned Aerial Vehicle Low-Altitude Remote Sensing (UAV-LARS) Use in Agricultural Monitoring in China. *Remote Sens* 13(6):1221. <https://doi.org/10.3390/rs13061221>
- Zong J, Zhu B, Hou Z, Yang X, Zhai J (2021) Evaluation and Comparison of Hybrid Wing VTOL UAV with Four Different Electric Propulsion Systems. *Aerospace* 8(9):256. <https://doi.org/10.3390/aerospace8090256>